JACS
JOURNAL OF THE AMERICAN CHEMICAL SOCIETY
Article
pubs.acs.org/JACS

Deep-Blue Phosphorescence from Perfluoro Carbonyl-Substituted Iridium Complexes

Sunghun Lee,[‡,†] Seul-Ong Kim,[§,†] Hyun Shin,[‡] Hui-Jun Yun,[§] Kiyull Yang,[⊥] Soon-Ki Kwon,*[,§] Jang-Joo Kim,*[,‡] and Yun-Hi Kim*[,¶]

[‡]WCU Hybrid Materials Program, Department of Materials Science and Engineering and the Center for Organic Light Emitting Diode, Seoul National University, Seoul 151-744, South Korea

[§]School of Materials Science and Engineering & Engineering Research Institute (ERI), [⊥]Department of Chemistry Education, and [¶]Department of Chemistry and Research Institute of Natural Sciences (RINS), Gyeongsang National University, Jinju, 660-701, South Korea

Supporting Information

ABSTRACT: The new deep-blue iridium(III) complexes, $(TF)_2Ir(pic)$, $(TF)_2Ir(fptz)$, $(HF)_2Ir(pic)$, and $(HF)_2Ir(fptz)$, consisting of 2′,4″-difluororphenyl-3-methylpyridine with trifluoromethyl carbonyl or heptafluoropropyl carbonyl at the 3′ position as the main ligand and a picolinate or a trifluoromethylated-triazole as the ancillary ligand, were synthesized and characterized for applications in organic light-emitting diodes (OLEDs). Density function theory (DFT) calculations showed that these iridium complexes had a wide band gap, owing to the introduction of the strong electron withdrawing perfluoro carbonyl group. Time-dependent DFT (TD-DFT) calculations suggested that their lowest triplet excited state was dominated by a HOMO → LUMO transition and that the contribution of the metal-to-ligand charge transfer (MLCT) was higher than 34% for all four complexes, indicating that strong spin−orbit coupling exists in the complexes. The 10 wt % $(TF)_2Ir(pic)$ doped 9-(3-(9*H*-carbazole-9-yl)phenyl)-3-(dibromophenylphosphoryl)-9*H*-carbazole (mCPPO1) film exhibited the highest photoluminescence quantum yield of 74 ± 3% among the films based on the four complexes. Phosphorescent OLEDs based on $(TF)_2Ir(pic)$ and $(TF)_2Ir(fptz)$ exhibited maximum external quantum efficiencies of 17.1% and 8.4% and Commission Internationale de l'Eclairage (CIE) coordinates of (0.141, 0.158) and (0.147, 0.116), respectively. These CIE coordinates represent some of the deepest blue emissions ever achieved from phosphorescent OLEDs with considerably high EQEs.

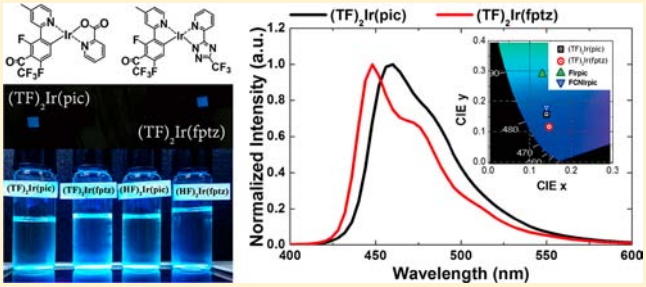

INTRODUCTION

Organic light-emitting diodes (OLEDs) have been successfully employed in small-sized displays and are being actively researched for application in large-sized, flexible displays and in solid-state lighting.[1] The efficiencies of OLEDs have been improved significantly owing to the adoption of phosphorescent emitters that can harvest triplet excitons as well as singlet excitons to produce light; thus, internal quantum efficiencies of nearly 100% have been achieved.[2−5] Red phosphorescent emitters that use iridium complexes have already been commercialized in small-sized OLEDs, and green iridium complexes are now competing with green fluorescent materials. In addition, research on the development of novel device structures that use exciplex-forming cohosts and phosphorescence dopants has shown that in the case of red, green, and even orange OLEDs, external quantum efficiencies (EQE) very close to the theoretical values reported in the literature (ca. 25−35%) can be achieved.[5] Further, significant efforts have been made to develop new blue phosphorescent emitters.[6,7] However, it is very difficult to synthesize blue phosphorescent materials that exhibit high color purity as well as high photoluminescence (PL) quantum yield (QY). The development of highly efficient deep-blue phosphorescent emitters is important for lowering power consumption in displays and solid-state lighting.

The fundamental strategies for achieving deep-blue emission from iridium complexes are the following: (1) lowering the level of the highest occupied molecular orbital (HOMO) of the electron-withdrawing groups and (2) increasing the level of the lowest unoccupied molecular orbital (LUMO) of the electron-donating group. It is well understood now that the HOMO is primarily localized on the phenyl part of the cyclometalated ligands and on iridium(III) ions, and the LUMO is mainly distributed on the pyridine part of the cyclometalated ligands.[8] We had previously shown that the position of the substituent in dimethylated iridium complexes affects the color purity and efficiency of the corresponding OLEDs.[9]

In this article, we report the design and fabrication of four new deep-blue iridium complexes, which consist of a perfluoro

Received: June 28, 2013
Published: September 2, 2013

   dx.doi.org/10.1021/ja4065188 | J. Am. Chem. Soc. 2013, 135, 14321−14328

Scheme 1. Schemes of the Four Iridium Complexes[a]

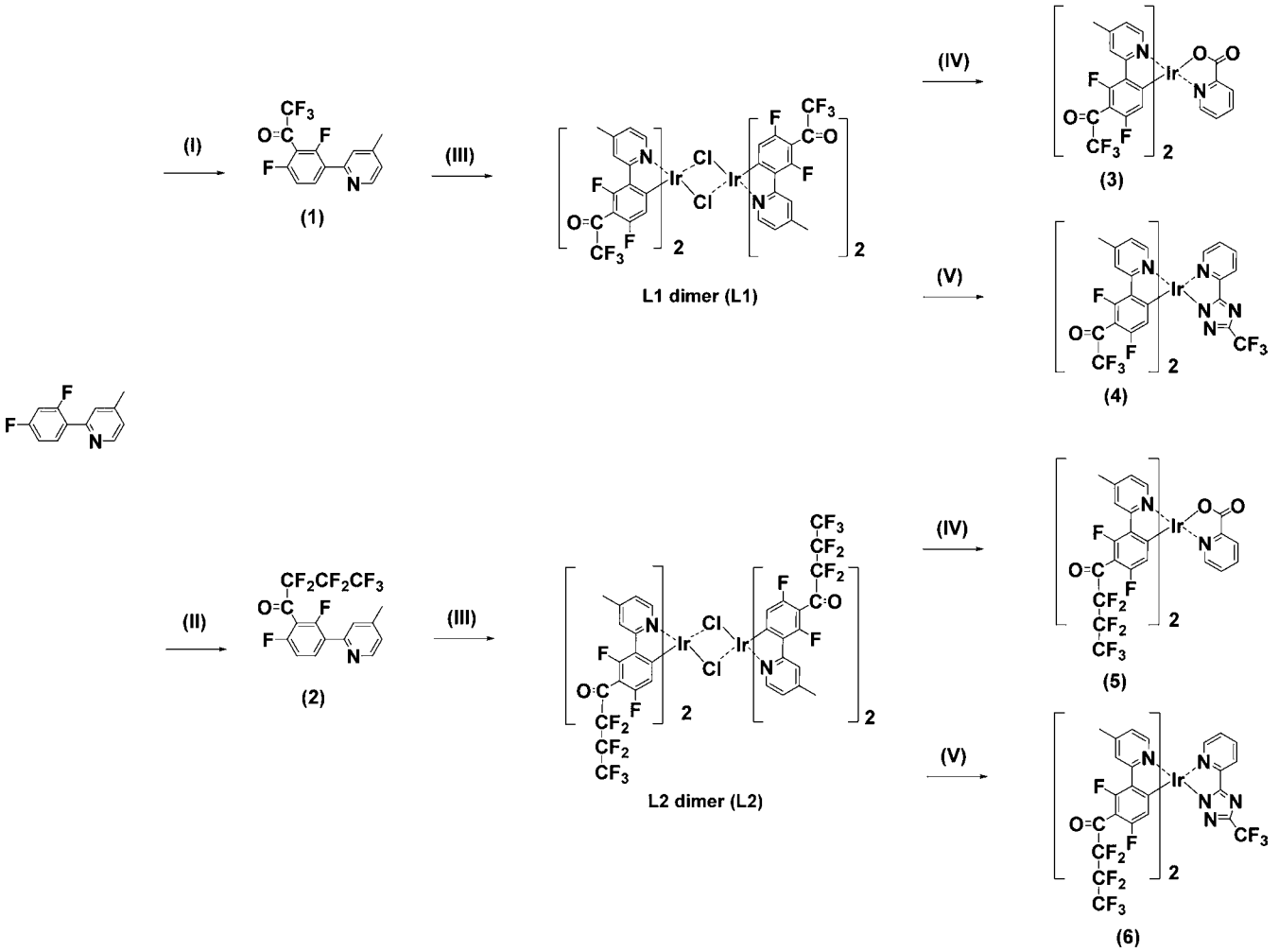

[a](I) LDA, ethyl 2,2,2-trifluoroacetate, ether, −78 °C; (II) LDA, ethyl 2,2,3,3,4,4,4-heptafluorobutanoate, ether, −78 °C; (III) $IrCl_3·H_2O$, 2-ethoxyethanol/H_2O, 100 °C, 24 h; (IV) picolinic acid, TBAOH, CH_2Cl_2, 30 °C, 8 h; (V) 2-(3-(trifluoromethyl)-1*H*-1,2,4-triazol-5-yl)pyridine, TBAOH, CH_2Cl_2, 30 °C, 8 h.

carbonyl substituent (a trifluoromethyl carbonyl or heptafluoropropyl carbonyl group) at the 3′ position of 2′,4″-difluororphenyl as a strong electron-withdrawing group that does not exhibit extended π-conjugation and a methyl group at the 4 position of the pyridine group. In particular, perfluoroalkyl carbonyl groups have several effects in Ir(III) cyclometalated complexes. One is a strong electron-withdrawing effect on the ligand π-system. Another is to provide steric protection around the metal; this is an important consideration for increasing the PL QY.[10] Moreover, fluorinated substituents in the aromatic ligands of metal complexes can be easily purified through sublimation under vacuum owing to their high volatility, resulting in high sublimation yields for commercial use. The ancillary ligand is also extended to include either a trifluoromethyl-substituted triazole or a picolinate as the ancillary ligand. It is known that C-linked 2-pyridyl-azoles are capable of using two adjacent nitrogen atoms to form a stable chelate. In addition, trifluoromethyl-substituted triazoles are strongly acidic; this was also reinforced further with the electron withdrawing the CF_3 substituent.[11]

In this study, we synthesized and characterized four new deep-blue iridium(III) complexes, which consisted of a trifluoromethyl carbonyl or heptafluoropropyl carbonyl group substituted at 2′,4″-difluororphenyl-3-methylpyridine as the main ligand and a picolinate or a trifluoromethylated triazole as the ancillary ligand. The CIE coordinates using four new iridium(III) complexes represent some of the deepest blue emissions ever achieved from phosphorescent OLEDs with considerably high EQEs.

■ RESULTS AND DISCUSSION

Two ligands, 1-(2,6-difluoro-3-(4-methylpyridin-2-yl)phenyl)-2,2,2-trifluoroethanone (TF) and 1-(2,6-difluoro-3-(4-methylpyridin-2-yl)phenyl)-2,2,3,3,4,4,4-heptafluorobutan-1-one (HF) (Scheme 1), were prepared from 2-(2,4-difluorophenyl)-4-methylpyridine and ethyl trifluoroacetate and 2-(2,4-difluorophenyl)-4-methylpyridine and ethyl heptafluorobutanoate, respectively, through one-step nucleophilic carbonyl substitution using lithium diisopropylamide (LDA) as a base. The 3′ position of 2′,4″-difluorophenyl was selected as the substitution position of the perfluoroalkyl carbonyl group based on density function theory (DFT) calculations revealing more blue shift at the 3′ position than the 5′ position as shown in Table S1 in Supporting Information.

dx.doi.org/10.1021/ja4065188 | J. Am. Chem. Soc. 2013, 135, 14321−14328

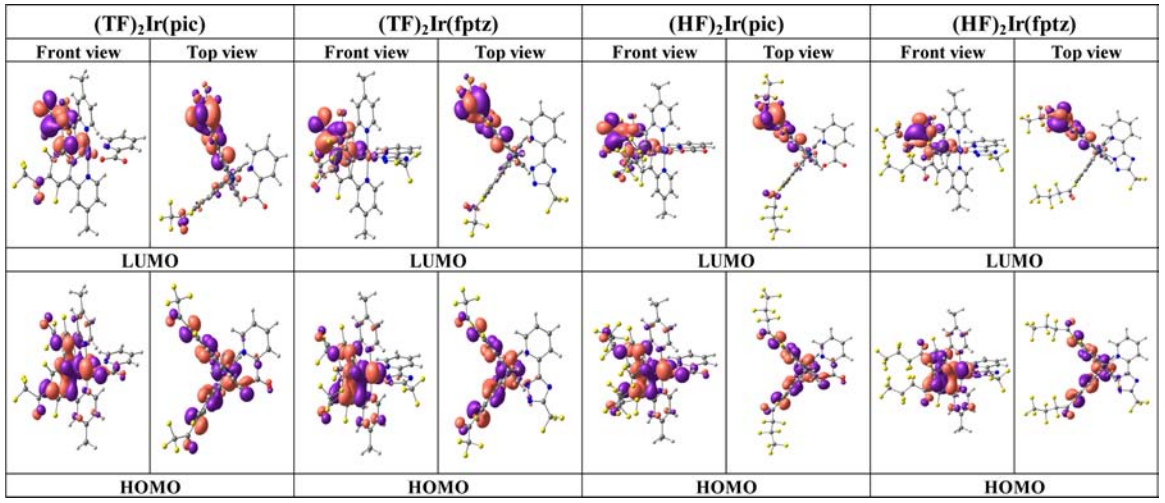

Figure 1. Contributions of the frontier molecular orbitals of the iridium complexes to the lowest triplet state, calculated using the density functional theory with B3LYP/6-31G as the base set.

A μ-chloro-bridged dimer was formed through the reaction of the cyclometalated ligand precursor with $IrCl_3 \cdot H_2O$ in a mixture of 2-ethoxyethanol and water. The new iridium complexes were obtained in the presence of tetrabutylammonium hydroxide via the reaction of the μ-chloro-bridged dimer and the ancillary ligand. The structures of these newly synthesized iridium complexes, $(TF)_2Ir(pic)$, $(TF)_2Ir(fptz)$, $(HF)_2Ir(pic)$, and $(HF)_2Ir(fptz)$, were characterized using NMR and high-resolution (HR) mass spectroscopies. (Scheme 1; Supporting Information)

Density function theory (DFT) calculations were performed in order to estimate the energy levels and electron density distributions of the orbitals of the four compounds using the B3LYP/6-31G as a base set for the ligands and the relativistic effective core potential of Los Alamos and Double-ξ basis sets (LANL2DZ)[12] for Ir (as implemented in Gaussian 03 package[13]). Time-dependent DFT (TD-DFT)[14] calculations were also performed to get singlet and triplet transition energies, on the basis of the structures optimized in their ground state. The optimized structures of and HOMO/LUMO levels for $(TF)_2Ir(pic)$, $(TF)_2Ir(fptz)$, $(HF)_2Ir(pic)$, and $(HF)_2Ir(fptz)$ are shown in Figure 1. The electrons in the HOMO orbitals of $(TF)_2Ir(pic)$, $(TF)_2Ir(fptz)$, $(HF)_2Ir(pic)$, and $(HF)_2Ir(fptz)$ were mostly distributed over the phenyl orbitals of the main ligand, with there being a large contribution from the d atomic orbital of iridium as well. This suggested that the introduction of the strong electron-withdrawing perfluoro carbonyl group led to a decrease in the HOMO levels. In addition, the oxygen lone-pair orbitals in picolinic acid in the ancillary ligand affect the HOMO levels of $(TF)_2Ir(pic)$ and $(HF)_2Ir(pic)$, while the triazole unit affects the HOMO levels of $(TF)_2Ir(fptz)$ and $(HF)_2Ir(fptz)$. As a result, the HOMO levels of $(TF)_2Ir(pic)$, $(TF)_2Ir(fptz)$, $(HF)_2Ir(pic)$, and $(HF)_2Ir(fptz)$ were calculated and found to be −6.33, −6.59, −6.37, and −6.62 eV, respectively. As expected, $(TF)_2Ir(fptz)$ and $(HF)_2Ir(fptz)$ with a trifluoro triazole as the ancillary ligand exhibited lower HOMO levels than did $(TF)_2Ir(pic)$ and $(HF)_2Ir(pic)$. In addition, $(HF)_2Ir(pic)$ and $(HF)_2Ir(fptz)$, which had the strong electron-withdrawing heptafluoropropyl carbonyl group, exhibited slightly lower HOMO levels than did $(TF)_2Ir(pic)$. However, electrons in the LUMO orbitals of the iridium complexes were distributed almost identically in the perfluoro carbonylated phenyl part of one of the main ligands. The LUMO levels of $(TF)_2Ir(pic)$, $(TF)_2Ir(fptz)$, $(HF)_2Ir(pic)$, and $(HF)_2Ir(fptz)$ were −2.73, −2.84, −2.87, and −2.96 eV, respectively. The compounds $(HF)_2Ir(pic)$ and $(HF)_2Ir(fptz)$, which had the strong electron-withdrawing heptafluoropropyl carbonyl group in the main ligand, exhibited lower LUMO levels than did $(TF)_2Ir(fptz)$. On the other hand, $(TF)_2Ir(fptz)$ and $(HF)_2Ir(fptz)$, which contained an electron-withdrawing triazole as the ancillary ligand, exhibited slightly lower LUMO levels than did $(TF)_2Ir(pic)$ and $(HF)_2Ir(pic)$, respectively. These results imply that the trifluoromethyl triazole unit lowers the HOMO levels of $(TF)_2Ir(fptz)$ and $(HF)_2Ir(fptz)$ significantly, leading to a larger band gap. On the other hand, the heptafluoropropyl carbonyl-substituted main ligand lowers the LUMO levels of $(HF)_2Ir(pic)$ and $(HF)_2Ir(fptz)$ significantly, leading to lower band gaps; this was in spite of the strong electron-withdrawing group. As a result, the band gaps could be arranged in the following order: $(HF)_2Ir(pic) < (TF)_2Ir(pic) < (HF)_2Ir(fptz) < (TF)_2Ir(fptz)$.

The contributions of the molecular orbitals to triplet transitions, determined from TD-DFT calculations, are shown in Table 1. The lowest triplet excited state for all the compounds was found to be dominated by a HOMO → LUMO transition. The triplet transition consists of a metal-to-ligand charge transfer (MLCT) (i.e., Ir→perfluoro phenyl fragment) transition and an interligand π (TF or HF) → π^*(TF or HF) transition with minor ligand-centered (LC) transitions as shown in Figure 1.

Table 1. Summary of the Contributions of the Frontier Molecular Orbitals of the Iridium Complexes to the Triplet Transitions As Determined Using TD-DFT Calculations

Ir complex	λ [nm]	assignment	MLCT [%]
$(TF)_2Ir(pic)$	T_1 466	HOMO→LUMO (80%)	37.80
$(TF)_2Ir(fptz)$	T_1 450	HOMO→LUMO (62%)	34.23
$(HF)_2Ir(pic)$	T_1 472	HOMO→LUMO (82%)	39.75
$(HF)_2Ir(fptz)$	T_1 453	HOMO→LUMO (72%)	37.62

Further, the contribution of the MLCT was calculated for the iridium complexes and was found to be higher than 34% for all

dx.doi.org/10.1021/ja4065188 | J. Am. Chem. Soc. 2013, 135, 14321−14328

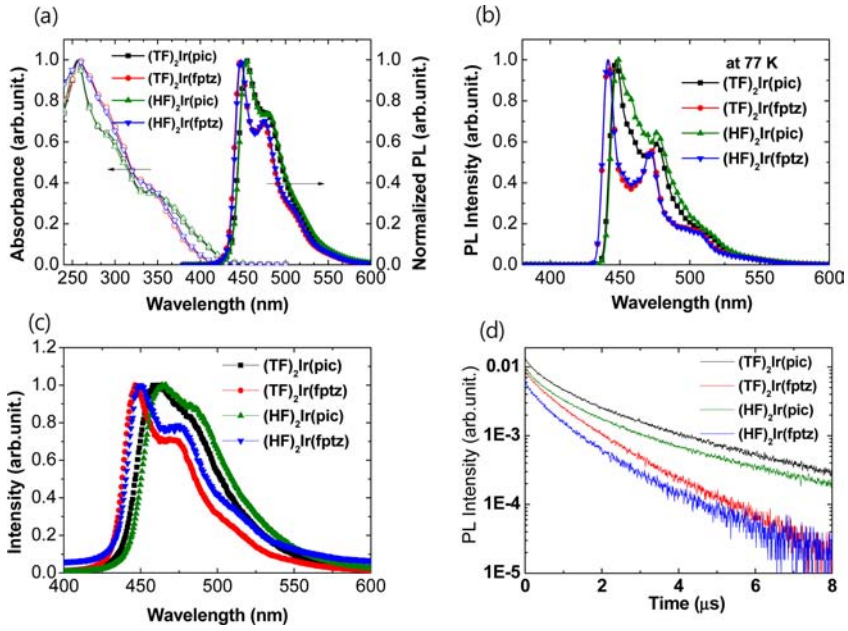

Figure 2. (a) UV−vis absorption and PL spectra of the iridium complexes in $CHCl_3$, (b) PL spectra at low temperature (77 K), (c) PL spectra of mCPPO1 films doped with the iridium complexes in the amount of 10 wt %, and (d) transient PL spectra of mCPPO1 films doped with the iridium complexes in the amount of 10 wt %.

four iridium complexes, indicating that strong spin−orbit coupling exists in the complexes.

The thermal stabilities of the iridium complexes were analyzed through differential scanning calorimetry (DSC) and thermogravimetric analysis (TGA) in a nitrogen atmosphere (Supporting Information, Figure S1). The 5% degradation temperatures (T_d) of the compounds were 380 °C for $(TF)_2Ir(pic)$, 372 °C for $(TF)_2Ir(fptz)$, 362 °C for $(HF)_2Ir(pic)$, and 368 °C for $(HF)_2Ir(fptz)$. The glass-transition temperature of $(HF)_2Ir(fptz)$ was 220 °C; $(TF)_2Ir(pic)$, $(TF)_2Ir(fptz)$, and $(HF)_2Ir(pic)$ did not undergo glass transition until they were heated to 250 °C. This was evidence of the thermal stability of the iridium complexes.

Figure 2a shows the ultraviolet−visible (UV−vis) absorption and PL spectra of the iridium complexes in a $CHCl_3$ solution at room temperature. The iridium complexes with the same ancillary ligand exhibit very similar absorption spectra, indicating that the ancillary ligands contribute significantly to the absorption process. The high-energy bands at approximately 257 and 264 nm in the case of the iridium complexes with the trifluoromethyl-substituted triazole and the picolinate ancillary ligands, respectively, were assigned to the respective intraligand $\pi-\pi^*$ transitions of the ligand.

The absorption bands at approximately 285 and 290 nm in the case of the iridium complexes with the trifluoromethyl-substituted triazole and the picolinate ancillary ligands, respectively, were indicative of spin-allowed ligand-centered absorptions. The spin-allowed ^{1}MLCT absorptions at approximately 347, 343, 352, and 347 nm could clearly be attributed to $(TF)_2Ir(pic)$, $(TF)_2Ir(fptz)$, $(HF)_2Ir(pic)$, and $(HF)_2Ir(fptz)$, respectively. Moreover, a spin-forbidden triplet ^{3}MLCT or ^{3}LC transitions or both appeared as low-energy absorption shoulders at approximately 420 and 430 nm in the case of the complexes with the trifluoromethyl-substituted triazole and the picolinate ancillary ligand, respectively. The phosphorescence spectra of the iridium complexes in the $CHCl_3$ solution at room temperature showed dominant phosphorescence emissions at approximately 440−500 nm, with maximas at 453 and 476 nm for (TF)2Ir(pic), 447 and 474 nm for (TF)2Ir(fptz), 454 and 479 nm for (HF)2Ir(pic), and 447 and 476 nm for (HF)2Ir(fptz).

The phosphorescence spectra of the iridium complexes in the $CHCl_3$ solution at 77 K are shown in Figure 2b. The absence of fine vibronic progressions in the phosphorescence spectra at 77 K indicates that the ^{3}MLCT excited state contributed significantly to the lowest excited triplet state of the iridium complexes.[15] However, the fact that the rigidochromic shift of the iridium complexes was small, ca. 5−6 nm, indicates that the phosphorescence was from the less polar excited state.[15] The PL QYs of the iridium complexes were measured using 9-(3-(9*H*-carbazole-9-yl)phenyl)-3-(dibromophenylphosphoryl)-9*H*-carbazole (mCPPO1) films doped with the iridium complexes in the amount of 10 wt %. An integrating sphere was used for the measurements. The PL QYs of $(TF)_2Ir(pic)$, $(HF)_2Ir(pic)$, and $(TF)_2Ir(fptz)$, $(HF)_2Ir(fptz)$ were determined to be 74 ± 3%, 52 ± 3%, 63 ± 3%, and 42 ± 3%, respectively. The PL spectra and transient PL of the doped films are shown in Figure 2c,d. The observed lifetimes of the iridium complexes were determined to be 2.71 μs, 2.74 μs, 1.46 μs, and 1.54 μs for $(TF)_2Ir(pic)$, $(HF)_2Ir(pic)$, $(TF)_2Ir(fptz)$, and $(HF)_2Ir(fptz)$, respectively. On the basis of the PL QYs and observed lifetimes of the iridium complexes, the radiative lifetimes of the complexes were deduced to be 3.7 μs, 5.3 μs, 2.3 μs, and 3.7 μs for $(TF)_2Ir(pic)$, $(HF)_2Ir(pic)$, $(TF)_2Ir(fptz)$, and $(HF)_2Ir(fptz)$, respectively. In addition, the values of their nonradiative decay rate constant (K_{nr}) were calculated and found to be 1.0×10^5 s^{-1}, 1.8×10^5 s^{-1}, 2.5×10^5 s^{-1}, and 3.8×10^5 s^{-1} for $(TF)_2Ir(pic)$, $(HF)_2Ir(pic)$, $(TF)_2Ir(fptz)$, and $(HF)_2Ir(fptz)$, respectively. The nonradiative decay rate constants of the iridium complexes with the same ancillary ligand were similar. This suggested that the fact that the PL QYs of the iridium complexes with the picolinate ligand were higher was mainly due to their nonradiative decay rate constants being lower than those of the iridium complexes

dx.doi.org/10.1021/ja4065188 | J. Am. Chem. Soc. 2013, 135, 14321−14328

Table 2. Photophysical and Electronic Properties of the Iridium Complexes

Ir complex	absorption[a] [nm]	PL[a] [nm]	PL[b] [nm]	fwhm[a] [nm]	rigidochromic shift[c] [nm]	T_1 [eV]	HOMO [eV]	E_g[d] [eV]	LUMO [eV]	PL[e] [nm]	QY[e] [%]	life time[e] [μs]	τ_r[e] [μs]	τ_{nr}[e] [μs]
$(TF)_2Ir(pic)$	257,290, 347	453, 476	447, 476	50	6	2.77	−5.9	2.9	−3.0	461, 483	74 ± 3	2.71	3.7	10.4
$(TF)_2Ir(fptz)$	264, 285, 343	447, 474	442, 472	46	5	2.81	−6.1	3.0	−3.1	446, 470	63 ± 3	1.46	2.3	3.9
$(HF)_2Ir(pic)$	257, 290, 352	454, 479	448, 476	50	6	2.77	−5.9	2.9	−3.0	464, 485	52 ± 3	2.74	5.3	5.7
$(HF)_2Ir(fptz)$	264, 285, 347	447, 476	442, 472	46	5	2.81	−6.1	3.0	−3.1	449, 474	42 ± 3	1.54	3.7	2.7

[a]Measured in a $CHCl_3$ solution at room temperature. [b]Measured in $CHCl_3$ solution at 77 K. [c]The difference between the PL peaks measured at room temperature and at 77 K. [d]Optical band gap. [e]Measured using 50-nm-thick mCPPO1films doped with the iridium complexes in the amount of 10 wt %.

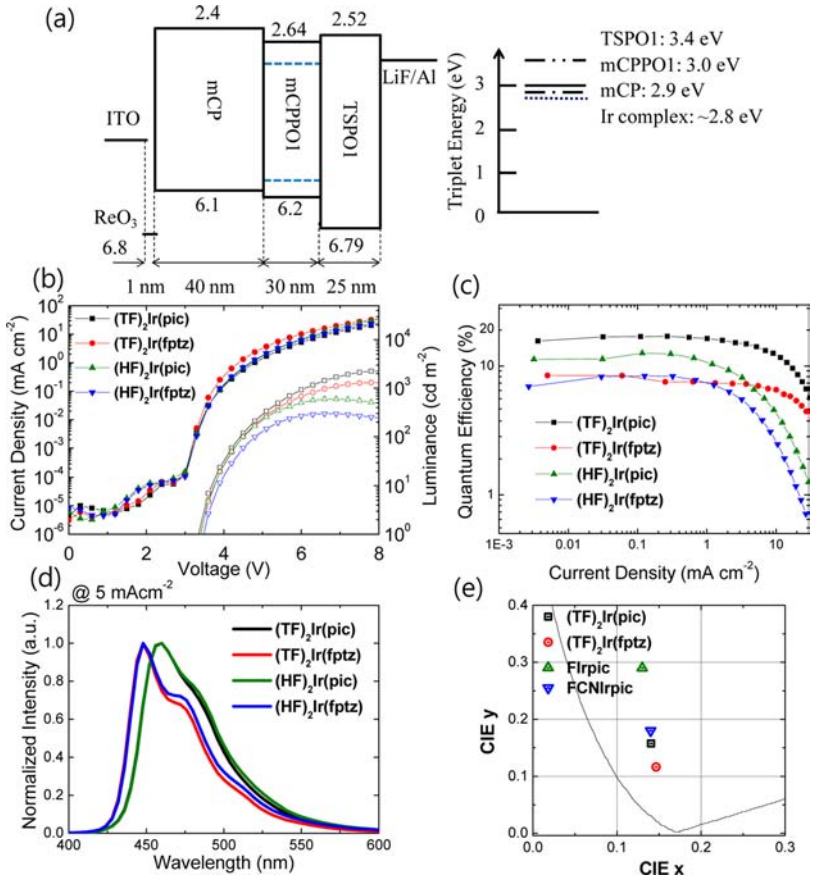

Figure 3. (a)Device structure, energy level diagrams of the OLEDs, and triplet energy levels of the constituent materials of the OLEDs. (b) Current density−voltage−luminance curves, (c) quantum efficiencies versus current density curves, and (d) normalized EL spectra of the different phosphorescent blue OLEDs at 5 mA cm^{-2}. (e) Comparison of the CIE coordinates of the EL from several blue phosphorescent OLEDs.

with the trifluoromethyl-substituted triazole as the ancillary ligand. The lower PL QYs of the iridium complexes with the heptafluoropropyl carbonyl substituent for the same ancillary ligand might originate from the nonradiative process from longer perfluoro carbonyl substitution than the iridium complexes with the trifluoromethyl carbonyl substitution. The HOMO levels of the iridium complexes were measured using cyclic voltammetry, and the LUMO levels of the materials were determined from their HOMO levels and optical band gaps, which were calculated from the UV−vis absorption spectra shown in Figure 2a. The photophysical and electronic properties of the iridium complexes are summarized in Table 2.

Phosphorescent blue OLEDs were fabricated using the iridium complexes as the dopants of a phosphorescent emitting layer. The device structure of the phosphorescent blue OLEDs was as follows: glass/indium tin oxide (ITO)/ReO_3(1 nm)/mCP (40 nm)/mCPPO1:iridium complexes (30 nm, 10 wt %)/TSPO1 (25 nm)/LiF (1 nm)/Al (100 nm), with mCP being *N*,*N*′-dicarbazolyl-3,5-benzene and TSPO1 being diphenylphosphine oxide-4-(triphenylsilyl)phenyl.

The device structure was a simple one and consisted of only three organic layers. A 1-nm-thick layer of ReO_3 was used as the hole injection layer because ReO_3 has a very high work function (6.8 eV), which effectively enhances the hole injection from ITO to mCP with deep HOMO level (−6.1 eV). The

dx.doi.org/10.1021/ja4065188 | J. Am. Chem. Soc. 2013, 135, 14321−14328

Table 3. Electroluminescence Characteristics of the Phosphorescent Blue OLEDs

	voltage [V]		EL_{max} [nm]	CIE (x, y)	EQE [%]			current efficiency [cd A^{-1}]		power efficiency [lm W^{-1}]	
Ir complex	turn-on[a]	@100 cd m^{-2}	@5 mA cm^{-2}	@5 mA cm^{-2}	max	@100 cd m^{-2}	@5 mA cm^{-2}	max	@100 cd m^{-2}	max	@100 cd m^{-2}
$(TF)_2Ir(pic)$	3.3	4.4	460	(0.141, 0.158)	17.1	16.83	14.88	21.7	21.31	19	15.20
$(TF)_2Ir(fptz)$	3.3	4.5	448	(0.147, 0.116)	8.4	7.36	7.24	8.6	7.53	8.1	5.25
$(HF)_2Ir(pic)$	3.3	4.5	460	(0.143, 0.169)	12.6	11.53	6.56	16.8	15.25	13.5	10.65
$(HF)_2Ir(fptz)$	3.4	4.8	448	(0.149, 0.130)	8.4	7.10	4.58	9.1	7.78	7.7	5.09

[a]Turn-on voltage at 1 cd m^{-2}.

mCP and TSPO1 layers functioned as the hole-transporting and electron-transporting layers, respectively. The compound mCPPO1 was chosen as the host material owing to its high triplet energy and because electron and hole mobilities in it are balanced.[16] As shown in Figure 3a, the LUMO level of mCPPO1 is 0.24 eV lower than that of mCP, and its HOMO level is 0.59 eV higher than that of TSPO1. As a result, the charge carriers are effectively confined within the emitting material layer (EML). Moreover, the triplet energy levels of all the constituent materials were higher than those of the iridium complexes; this effectively confined the triplet excitons within the EML.

Figure 3b shows the current density−voltage−luminance (J−V−L) characteristics of the OLEDs. The turn-on voltage for all four OLEDs was 3.3 V. The J−V characteristics of all four devices were similar because they had the same structure. However, the L−V characteristics of the OLEDs based on the iridium complexes with trifluoromethyl carbonyl substitution were different from those based on the complexes with heptafluoropropyl carbonyl substitution. The devices based on the iridium complexes with the heptafluoropropyl carbonyl substituent showed lower maximum luminances than did the devices based on the complexes with the trifluoromethyl carbonyl substituent. This might be owing to the instability of the bulky heptafluoropropyl carbonyl units. The external quantum efficiency−current density (EQE−J) characteristics of the OLEDs are shown in Figure 2c. The device with $(TF)_2Ir(pic)$ shows the highest EQE among all the devices; this was expected, given that the PL QY of $(TF)_2Ir(pic)$ was the highest. However, the maximum EQE of the device with $(TF)_2Ir(fptz)$ was lower than that of the device with $(HF)_2Ir(pic)$ and similar to that of the device with $(HF)_2Ir(fptz)$, even though the PL QY of $(TF)_2Ir(fptz)$ is higher than that of $(HF)_2Ir(pic)$ and $(HF)_2Ir(fptz)$. This was because the device structure was more optimized for $(HF)_2Ir(pic)$ and $(HF)_2Ir(fptz)$ than it was for $(TF)_2Ir(fptz)$. The higher EQE of the device with $(HF)_2Ir(pic)$ can be explained on the basis of the fact that the device structure employed was optically more optimized for emissions of longer wavelengths such as those from $(TF)_2Ir(pic)$ and $(HF)_2Ir(pic)$. In addition, we speculate that the difference between the EQE values of the devices with $(TF)_2Ir(fptz)$ and $(HF)_2Ir(fptz)$ arises from the fact that the introduction of the trifluoromethyl-substituted triazole ligand and the trifluoromethyl carbonyl substitution together result in a negative charge balance in the EML. The maximum EQEs were 17.1, 8.4, 12.6, and 8.4% and the EQEs at 5 mA cm^{-2} were 14.9, 7.2, 6.6, and 4.6% for the devices with $(TF)_2Ir(pic)$, $(TF)_2Ir(fptz)$, $(HF)_2Ir(pic)$, and $(HF)_2Ir(fptz)$, respectively. The extremely high efficiency roll-off at a high current density in the case of the devices with $(HF)_2Ir(pic)$ and $(HF)_2Ir(fptz)$ was due to the instability of the iridium complexes, as mentioned before. However, the efficiency roll-off at high current density in the case of the devices based on $(TF)_2Ir(pic)$ and $(TF)_2Ir(fptz)$ was similar to that of phosphorescent OLEDs.[2,3,15] The performance parameters of the four OLEDs are summarized in Table 3.

The color purity of phosphorescent blue OLEDs is highly important since it is difficult to achieve deep-blue phosphorescent emissions. There are only a limited number of blue dopants that can emit blue radiation with a y value (C_y) lower than 0.2 in the 1931 Commission Internationale de L'Éclairage (CIE) chromaticity diagram while also exhibiting a high EQE,[17] which are summarized Table S2 in Supporting Information. The electroluminescence (EL) spectra of the four devices at 5 mA cm^{-2} are shown in Figure 3d. The emission peak (EL_{max}) of the OLEDs based on $(TF)_2Ir(pic)$ and $(HF)_2Ir(pic)$, was located at 460 nm, while that of the device based on $(TF)_2Ir(fptz)$ and $(HF)_2Ir(fptz)$, was located at 448 nm. The values of the full width at half-maximum (fwhm) of all four devices were less than 50 nm. Owing to the spectral purities of the emissions from the OLEDs, the CIE coordinates (x,y) of the devices with $(TF)_2Ir(pic)$, $(TF)_2Ir(fptz)$, $(HF)_2Ir(pic)$, and $(HF)_2Ir(fptz)$ at 5 mA cm^{-2} were (0.141, 0.158), (0.147, 0.116), (0.143, 0.169), and (0.149, 0.130), respectively. Figure 3e shows a comparison of the 1931 CIE coordinates of the devices with $(TF)_2Ir(pic)$ and $(TF)_2Ir(fptz)$ and representative high-EQE blue phosphorescent devices based on the extensively studied dopants [iridium(III) bis(4,6-difluorophenyl)-pyridinato-N,C']picolinate (FIrpic) and bis((3,5-difluoro-4-cyanophenyl)pyridine) iridium(III) picolinate (FCNIrpic).[16,18] The $(TF)_2Ir(pic)$ and $(TF)_2Ir(fptz)$ devices exhibited lower CIE C_y values than those of the FIrpic and FCNIrpic devices.

CONCLUSIONS

Four new deep-blue iridium(III) complexes, $(TF)_2Ir(pic)$, $(TF)_2Ir(fptz)$, $(HF)_2Ir(pic)$ and $(HF)_2Ir(fptz)$, consisting of a trifluoromethyl carbonyl or heptafluoropropyl carbonyl group substituted at 2′,4″-difluororphenyl-3-methylpyridine as the main ligand and a picolinate or trifluoromethylated triazole as the ancillary ligand, were successfully synthesized and characterized. These iridium complexes exhibited wide band gaps, as determined by DFT calculations, due to the introduction of the strong electron-withdrawing perfluoro carbonyl group. Moreover, TD-DFT calculations showed that the lowest triplet excited states of the complexes were dominated by a HOMO → LUMO transition, and the

dx.doi.org/10.1021/ja4065188 | J. Am. Chem. Soc. 2013, 135, 14321−14328

contribution of the MLCT was greater than 34% for all the iridium complexes. This indicated that strong spin−orbit coupling exists in the complexes. Phosphorescent OLEDs based on $(TF)_2Ir(pic)$ and $(TF)_2Ir(fptz)$ exhibited high maximum EQEs of 17.1 and 8.4% and CIE coordinates of (0.141, 0.158) and (0.147, 0.116), respectively. These CIE coordinates represent some of the deepest blue emissions ever achieved from phosphorescent OLEDs with considerably high EQEs.[17]

EXPERIMENTAL SECTION

Materials. All reagents and solvents used for the experiment were purchased from Aldrich and TCI and were used without further purification. All the synthesized materials were purified using train sublimation with the yield over 60%.

Material Characterization. IR spectra were recorded using a Genesis II FT-IR spectrometer. ^1H NMR was recorded using Avance 300 MHz NMR Bruker spectrometers, and chemical shifts are reported in ppm units with tetramethylsilane as the internal standard. Thermogravimetric analysis (TGA) was performed under nitrogen on a TA Instruments 2050 thermogravimetric analyzer. The sample was heated at 10 °C·min^{-1} from 50 to 700 °C. The differential scanning calorimeter (DSC) was conducted under nitrogen in a TA Instruments 2100 differential scanning calorimeter. The sample was heated at 10 °C·min^{-1} from 30 to 350 °C. Mass spectra were measured using a Jeol JMS-700 mass spectrometer. UV−vis absorption spectra were measured using a Perkin-Elmer LAMBDA-900 UV−vis−NIR spectrophotometer and an LS-50B luminescence spectrophotometer, respectively. The cyclic voltammogram of the material was recorded on an epsilon E3 at room temperature in a 0.1-M solution of tetrabutylammonium perchlorate (Bu_4NClO_4) in acetonitrile under nitrogen gas at a scan rate of 50 mV/s. A Pt wire was used as the counter electrode and an $Ag/AgNO_3$ electrode as the reference electrode.

Device Fabrication and Characterization. Photophysical study and device fabrication and evaluation: The 50-nm-thickness 10 wt % iridium complexes doped mCPPO1 films for the measurement of the PL QYs and transient PL were fabricated by thermal evaporation on precleaned fused silica substrates at a base pressure less than 5×10^{-7} Torr. The PL QYs of the organic films were measured using an integrating sphere. A continuous-wave He/Cd laser (325 nm) was used as an excitation light source, and a monochromator attached photomultiplier tube (PMT) was used as an optical detector system. The PL spectra were measured using a pulsed Nd−YAG laser (355 nm) as the excitation light source and an intensified charge-coupled device as the optical detector for the PL measurements. For the transient PL measurement, a pulsed Nd−YAG laser (355 nm) was used as the excitation light source and a monochromator attached PMT was used as an optical detector system to get the lifetimes of the films. Detection wavelengths for $(TF)_2Ir(pic)$, $(TF)_2Ir(fptz)$, $(HF)_2Ir(pic)$, and $(HF)_2Ir(fptz)$ were 460, 447, 465, and 450 nm which correspond to the peak wavelengths of the films, respectively. All signals were detected and integrated 1000 times by an oscilloscope (54642A, Agilent). The OLEDs were fabricated by thermal evaporation onto cleaned glass substrates precoated and prepatterned with 70 nm-thick indium tin oxide (ITO). Prior to the deposition of organic layers, the ITO substrates were exposed to a UV−ozone flux for 10 min following degreasing in acetone and isopropylalcohol. Organic and metal layers were deposited by thermal evaporation at the base pressure < 5×10^{-7} Torr without breaking vacuum. The current density and the luminance were measured using a Keithley 2400 programmable source meter and a Minolta CS 100 (Minolta) and the EL spectra were measured using SpectraScan PR650 (Photo Research). The EQEs of the OLEDs were calculated from the current density, the luminance, and the EL spectra using the Lambertian angular distribution approximation.

ASSOCIATED CONTENT

Supporting Information

Synthesis and characterization details; TGA and DSC thermograms data. This material is available free of charge via the Internet at http://pubs.acs.org.

AUTHOR INFORMATION

Corresponding Authors

skwon@gnu.ac.kr
jjkim@snu.ac.kr
ykim@gnu.ac.kr

Author Contributions

†S.L. and S.-O.K. contributed equally to this work.

Notes

The authors declare no competing financial interest.

ACKNOWLEDGMENTS

This work was supported by the Industrial Strategic Technology Development Program [10035225, Development of core technology for high performance AMOLED on plastic] funded by MKE/KEIT, supported by Nanomaterial Technology of NRF (2012049647), and supported by Samsung display.

REFERENCES

(1) (a) Baldo, M. A.; O'Brien, D. F.; You, Y.; Shoustikov, A.; Sibley, S.; Thompson, M. E.; Forrest, S. R. *Nature* **1998**, *393*, 151. (b) Baldo, M. A.; Thompson, M. E.; Forrest, S. R. *Nature* **2000**, *403*, 750. (c) Reineke, S.; Linder, F.; Schwartz, G.; Seidler, N.; Walzer, K.; Lussem, B.; Leo, K. *Nature* **2009**, *459*, 234. (d) Chi, Y.; Chou, P.-T. *Chem. Soc. Rev.* **2010**, *39*, 638.

(2) Adachi, C.; Baldo, M. A.; Thompson, M. E.; Forrest, S. R. *J. Appl. Phys.* **2001**, *90*, 5048.

(3) Yang, C. H.; Cheng, Y. M.; Chi, Y.; Hsu, C. J.; Fang, F. C.; Wong, K. T.; Chou, P. T.; Chang, C. H.; Tsai, M. H.; Wu, C. C. *Angew. Chem. Int. Ed.* **2007**, *46*, 2418.

(4) (a) Park, Y.-S.; Kang, J.-W.; Kang, D. M.; Park, J.-W.; Kim, Y.-H.; Kwon, S.-K.; Kim, J.-J. *Adv. Mater.* **2008**, *20*, 1957. (b) Leem, D.-S.; Jung, S. O.; Kim, S.-O.; Park, J.-W.; Kim, J. W.; Park, Y.-S.; Kim, Y.-H.; Kwon, S. K.; Kim, J.-J. *J. Mater. Chem.* **2009**, *19*, 8824. (c) Kang, D. M.; Park, J. W.; Jung, S. O.; Lee, S. H.; Park, H. D.; Kim, Y. H.; Shin, S. C.; Kim, J.-J.; Kwon, S. K. *Adv. Mater.* **2008**, *20*, 2003. (e) Tanaka, D.; Sasabe, H.; Li, Y.-J.; Su, S.-J.; Takeda, T.; Kido, J. *Jpn. J. Appl. Phys.* **2007**, *46*, L10. (f) Helander, M. G.; Wang, Z. B.; Qiu, J.; Greiner, M. T.; Puzzo, D. P.; Liu, Z. W.; Lu, Z. H. *Science* **2011**, *332*, 944.

(5) (a) Park, Y.-S.; Lee, S.; Kim, K.-H.; Kim, S.-Y.; Lee, J.-H.; Kim, J.-J. *Adv. Funct. Mater.* **2013**, DOI: 10.100/adfm.201300547. (b) Kim, S.-Y.; Jeong, W.-I.; Mayr, C.; Park, Y.-S.; Kim, K.-H.; Lee, J.-H.; Moon, C.-K.; Brütting, W.; Kim, J.-J. *Adv. Funct. Mater.* **2013**, *23*, 3896. (c) Lee, S.; Kim, K.-H.; Limbach, D.; Park, Y.-S.; Kim, J.-J. *Adv. Funct. Mater.* **2013**, *23*, 4105. (d) Lee, S.; Limbach, D.; Kim, K.-H.; Park, Y.-S.; Kim, J.-J. *Org. Electron.* **2013**, *14*, 1856. (e) Kim, K.-H.; Lee, S.; Kim, S.-Y.; Park, Y.-S.; Lee, J.-H.; Huh, J.; You, Y.; Kim, J.-J., 2013, unpublished.

(6) (a) Homes, J. R.; D'Andrade, B. W.; Forrest, S. R.; Ren, X.; Li, J.; Thompson, M. E. *Appl. Phys. Lett.* **2003**, *83*, 3818. (b) Yeh, S. J.; Wu, M. F.; Chen, C. T.; Song, Y. H.; Chi, Y.; Ho, M. H.; Chen, S. F.; Hsu, C. H. *Adv. Mater.* **2005**, *17*, 285. (c) Seo, H. L.; Yoo, K. M.; Song, M.; Park, J. S.; Jin, S. H.; Kim, Y. I.; Kim, J.-J. *Org. Electron.* **2010**, *11*, 564. (d) Sajoto, T.; Djurovich, P. I.; Tamayo, A. B.; Oxgaard, J.; Goddard, W. A.; Thomson, M. E. *J. Am. Chem. Soc.* **2008**, *131*, 9813. (e) Chiu, Y. C.; Hung, J. Y.; Chi, Y.; Pai, I.-H.; Yu, Y. C.; Lee, G. H.; Chou, P. T. *Adv. Mater.* **2009**, *21*, 2221. (f) Yang, C. H.; Cheng, Y.-M.; Chi, Y.; Chiu, Y. C.; Lin, C.-C.; Lee, G.-H.; Chou, P.-T.; Chen, C.-C.; Chang, C.-H.; Wu, C.-C. *Angew. Chem., Int. Ed.* **2008**, *120*, 4618. (g) Sasabe, H.; Takamatsu, J.; Motoyama, T.; Watanabe, S.; Wagenblast, G.; Langer, N.; Molt, O.; Fuchs, E.; Lennartz, C.; Kido, J. *Adv. Mater.*

2010, *22*, 5003. (h) Yang, C.-H.; Mauro, M.; Polo, F.; Watanabe, S.; Muenster, I.; Frohlich, R.; Cola, L. D. *Chem. Mater.* **2012**, *24*, 3684. (i) Fan, C.; Li, Y.; Yang, C.; Wu, H.; Qin, J.; Cao, Y. *Chem. Mater.* **2012**, *24*, 4581. (j) Kim, C. Y.; Ha, D. G.; Kang, H. H.; Yun, H.-J.; Kwon, S. K.; Kim, J.-J.; Kim, Y. H. *J. Mater. Chem.* **2012**, *22*, 22721.

(7) (a) Yook, K. S.; Jeon, S. O.; Joo, C. W.; Lee, J. Y. *Org. Electron* **2009**, *10*, 170. (b) Jeon, S. O.; Yook, K. S.; Joo, C. W.; Lee, J. Y. *Adv. Funct. Mater.* **2009**, *19*, 3644. (c) Kim, S. H.; Jang, J.; Lee, S. J.; Lee, J. Y. *Thin Solid Films* **2008**, *517*, 722.

(8) Hay, P. J. *J. Phys. Chem. A* **2002**, *06*, 1634.

(9) Jung, S. O.; Kang, Y.; Kim, H. S.; Kim, Y. H.; Lee, C. L.; Kim, J.-J.; Kwon, S. K. *Eur. J. Inorg. Chem.* **2004**, *17*, 3415.

(10) Grushin, V. V.; Herron, N.; LeCloux, D. D.; Marshall, W. J.; Petrov, V. A.; Wang, Y. *Chem. Commun.* **2001**, 1494.

(11) (a) Kim, S.-O.; Zhao, Q.; Thangaraju, K.; Kim, J.-J.; Kim, Y.-H.; Kwon, S.-K. *Dyes Pigm.* **2011**, *90*, 139. (b) Mi, B. X.; Wang, P. F.; Gao, Z. Q.; Lee, C. S.; Lee, S. T.; Hong, H. L.; Chen, X. M.; Wong, M. S.; Xia, P. F.; Cheah, K. W.; Chen, C. H.; Huang, W. *Adv. Mater.* **2009**, *21*, 339. (c) Ulbricht, C.; Beyer, B.; Friebe, C.; Winter, A.; Schubert, U. S. *Adv. Mater.* **2009**, *21*, 4418. (d) Song, Y. H.; Chiu, Y. C.; Chi, Y.; Cheng, Y. M.; Lai, C. H.; Chou, P. T.; Wong, K. T.; Tsai, M. H.; Wu, C. C. *Chem.—Eur. J.* **2008**, *14*, 5423. (e) Pommerehne, J.; VestWeber, H.; Guss, W.; Mahrt, R. F.; Bassler, H.; Porsch, M.; Daub, J. *Adv. Mater.* **1995**, *7*, 551. (f) Thelakkat, M.; Schmidt, H. W. *Adv. Mater.* **1998**, *10*, 219. (g) Zhang, X. W.; Gao, J.; Yang, C. L.; Zhu, L. N.; Li, Z. A.; Zhang, K.; Qin, J. G.; You, H.; Ma, D. G. *J. Organomet. Chem.* **2006**, *691*, 4312.

(12) Hay, P. J.; Wadt, W. R. *J. Chem. Phys.* **1985**, *82*, 299.

(13) Frisch, M. J.; Trucks, G. W.; Schlegel, H. B.; Scuseria, G. E.; Robb, M. A.; Cheeseman, J. R.; Montgomery, J. A., Jr.; Vreven, T.; Kudin, K. N.; Burant, J. C.; Millam, J. M.; Iyengar, S. S.; Tomasi, J.; Barone, V.; Mennucci, B.; Cossi, M.; Scalmani, G.; Rega, N.; Petersson, G. A.; Nakatsuji, H.; Hada, M.; Ehara, M.; Toyota, K.; Fukuda, R.; Hasegawa, J.; Ishida, M.; Nakajima, T.; Honda, Y.; Kitao, O.; Nakai, H.; Klene, M.; Li, X.; Knox, J. E.; Hratchian, H. P.; Cross, J. B.; Bakken, V.; Adamo, C.; Jaramillo, J.; Gomperts, R.; Stratmann, R. E.; Yazyev, O.; Austin, A. J.; Cammi, R.; Pomelli, C.; Ochterski, J. W.; Ayala, P. Y.; Morokuma, K.; Voth, G. A.; Salvador, P.; Dannenberg, J. J.; Zakrzewski, V. G.; Dapprich, S.; Daniels, A. D.; Strain, M. C.; Farkas, O.; Malick, D. K.; Rabuck, A. D.; Raghavachari, K.; Foresman, J. B.; Ortiz, J. V.; Cui, Q.; Baboul, A. G.; Clifford, S.; Cioslowski, J.; Stefanov, B. B.; Liu, G.; Liashenko, A.; Piskorz, P.; Komaromi, I.; Martin, R. L.; Fox, D. J.; Keith, T.; Al-Laham, M. A.; Peng, C. Y.; Nanayakkara, A.; Challacombe, M.; Gill, P. M. W.; Johnson, B.; Chen, W.; Wong, M. W.; Gonzalez, C.; Pople, J. A. *Gaussian 03*, revision D.02; Gaussian, Inc.: Wallingford, CT, 2004.

(14) Casida, M. E.; Jamorski, C.; Casida, K. C.; Salahub, D. R. *J. Chem. Phys.* **1998**, *108*, 4439.

(15) Tsuboyama, A.; Iwawaki, H.; Furugori, M.; Mukaide, T.; Kamatani, J.; Igawa, S.; Moriyama, T.; Miura, S.; Takiguchi, T.; Okada, S.; Hoshino, M.; Ueno, K. *J. Am. Chem. Soc.* **2003**, *125*, 12971.

(16) Jeon, S. O.; Jang, S. E.; Son, H. S.; Lee, J. Y. *Adv. Mater.* **2011**, *23*, 1436.

(17) Yook, K. S.; Lee, J. Y. *Adv. Mater.* **2012**, *24*, 3169.

(18) Bin, J.-K.; Cho, N.-S.; Hong, J.-I. *Adv. Mater.* **2012**, *24*, 2911.